This is a repository copy of *Determination of dynamic surface tension and viscosity of non-Newtonian fluids from drop oscillations*.

White Rose Research Online URL for this paper:
http://eprints.whiterose.ac.uk/82344/

Version: Accepted Version

Determination of Dynamic Surface Tension and Viscosity of Non-Newtonian Fluids from Drop Oscillations

Lisong Yang[1], Bethany K. Kazmierski[1], Stephen D. Hoath[2], Sungjune Jung [2+], Wen-Kai Hsiao[2], Yiwei Wang[3++], Arganthaël Berson[4], Oliver Harlen[5], Nik Kapur[3] and Colin D. Bain[1*]

1. Department of Chemistry, Durham University, Durham DH1 3LE, UK
2. Department of Engineering, University of Cambridge, Cambridge CB3 0FS, UK
3. School of Engineering and Computing Sciences, Durham University, Durham DH1 3LE, UK
4. School of Mechanical Engineering, University of Leeds, Leeds LS2 9JT, UK
5. Faculty of Mathematics and Physical Sciences, University of Leeds, Leeds, LS2 9JT, UK

+ Current affiliation: Department of Creative IT Engineering, Pohang University of Science and Technology, Korea

++ Current affiliation: GlaxoSmithKline Plc, Barnard Castle, County Durham, DL12 8DT, UK

* Corresponding author. E-mail: c.d.bain@durham.ac.uk

Abstract

The oscillations of free-falling drops with size range from pL to μL have been used to measure the transient shear viscosity and the dynamic surface tension of shear-thinning fluids on the timescale of $10^{-5} - 10^{-2}$ s. The method is first validated with Newtonian fluids. For a given surface tension, the lower and upper limits for accurate measurement of the viscosity are determined as a function of drop size. The dynamic properties of two types of shear-thinning fluids with varying viscoelasticity are reported: aqueous suspensions of the antifungal drug griseofulvin and of the OLED material PEDOT: PSS. In both cases, the free-falling drop retains the high-shear viscosity.

Keywords: drop oscillation, dynamic surface tension, shear viscosity, shear thinning fluid, PEDOT:PSS, griseofulvin

1. Introduction

The oscillatory motion of a drop is a classical problem in fluid mechanics which has been studied for more than a century.[1-6] The technological importance of drop oscillations has been explored in applications such as sprays, inkjet printing, nuclear physics and meteorology.[7-10] Lord Rayleigh was the first to investigate mathematically the free oscillations of a drop and he derived a solution for small amplitude, axisymmetric oscillations of an inviscid and incompressible drop free from the influence of an outer fluid.[1] The instantaneous deformation of the droplet about its spherical shape is described by an infinite series of orthogonal surface spherical harmonics, i.e. the natural oscillation modes. The axisymmetric form is

$$r(\theta, t) = a_0 \left[1 + \sum_{l=2}^{\infty} a_l(t) P_l(\cos\theta) \right],$$ (1)

where $P_l(\cos\theta)$ are the Legendre polynomials of the order l, $a_l(t)$ is the instantaneous amplitude of the lth mode of oscillation, and θ is the polar angle of a spherical coordinate system with its origin at the centre of the spherical drop. For small amplitude oscillations, a_0 is the equilibrium radius of the droplet, r_0. The linear solution of the problem shows that the angular frequency Ω_l of the lth oscillation mode is given by

$$\Omega_l^2 = \sigma \frac{l(l-1)(l+2)}{\rho r_0^3},$$ (2)

where σ and ρ are the fluid's surface tension and density, respectively.

Later, more generalised linear analyses were developed which included the viscosity of the droplet and viscous effects of an outer fluid. Lamb obtained an irrotational solution for an oscillating drop with low viscosity and small oscillation amplitude.[2] The amplitude of the lth mode decays away exponentially with a decay time, τ_l, and an angular frequency of oscillation, Ω_l^*, given by

$$\tau_l = \frac{\rho r_0^2}{\mu(l-1)(2l+1)}$$ (3)

and $\Omega_l^* = \Omega_l \sqrt{1 - (\Omega_l \tau_l)^{-2}}$, (4)

where μ is the viscosity of the fluid. The effect of viscous dissipation is to reduce the oscillation frequency from the Rayleigh frequency. Prosperetti pointed out that the approximation given by Eqs. (2)–(4) is valid for Ohnesorge number $Oh = \mu/(\rho\sigma r_0)^{1/2}$ of < 0.1.[4]

The oscillating drop (OD) method has attracted great interest over decades for the determination

of the dynamic surface tension (DST) and viscosity of fluids. One approach is to look at free-falling drop immediately after its formation from orifice.[11-15] Trinh *et al.*[13] and Hiller and Kowalewski[14] studied freely oscillating drops with small oscillation amplitudes experimentally and validated the OD theory within the linear approximation for the fundamental mode. Stückrad *et al.* used the OD method to determine the temporal development of the DST of heptanol-water solutions and interpreted the results by a diffusion-controlled adsorption mechanism.[15] Becker *et al.* experimentally and theoretically investigated the nonlinear dynamics of viscous droplets with large initial amplitudes of oscillation, exceeding 10% of the drop radius for the fundamental mode. They found that nonlinear effects were most evident for higher oscillation modes ($l > 2$) while the fundamental mode conformed to the linear theory even for initial amplitudes exceeding 50% of the drop radius.[16] Matsumoto *et al.* developed a precise OD method based on levitated drops. [17]

The classical OD work cited above was restricted to Newtonian liquids. In recent years, the dynamic properties of complex fluids, such as polymer solutions, colloids, emulsions, gels and foams, have become of great interest both in fundamental research and for industrial applications involving jets, sprays and coatings. Khismatullin and Nadim[6] and Brenn and Teichtmeister[18] have developed theoretical treatments of oscillating viscoelastic drops and the latter authors recently reported a proof-of-concept experiment to measure polymer relaxation times in viscoelastic levitated drops. This approach is very promising for studying rheological properties of fluids close to equilibrium. The viscosity of complex fluids frequently depends not only on the rate of strain (non-Newtonian behaviour) but also on the shear history (thixotropy or rheopexy). Particle-laden fluids, such as oral pharmaceuticals and paints, are formulated to have a yield stress to prevent sedimentation during storage. Viscoelasticity may also be desirable to inhibit splashing on impact or the formation of fine aerosols. For such fluids, steady-state or low-amplitude oscillating shear measurements may not reflect the rheological behavior of a fluid under the conditions encountered during processing or final application. A particular example is the behavior of drops formed in a jet or a spray, where the fluid changes from the high-shear environment of a nozzle to the low-shear environment of a free drop over a period of microseconds to milliseconds. To predict the behavior of such droplets in flight or during impact, one needs to understand how the rheology evolves following a step-change in shear. The typical mechanical response of commercial rheometer switching between a high shear rate of, say, 1000 s^{-1} and low shear rate of 0.1 s^{-1} is a few tenths of a second, which is too slow to capture the

3

rheological behavior of drops in applications such as inkjet printing or spray painting. From a fundamental perspective, it is also desirable to have a direct measurement of transient shear viscosity of a fluid after a shear quench in order to understand the relationship between microstructure and macroscopic flow properties, for example, the network recovery in a colloidal suspension. Here we show that the OD method can be used to determine the transient shear viscosity of shear-thinning fluids on the timescale of a few tens of microseconds (for picolitre droplets) to a few tens of milliseconds (for microlitre drops) after the fluid leaves the high-shear environment inside the pipe and forms a drop in the low-shear environment of free space. Since the droplets themselves are used to interrogate the rheology, the shear history can be identical to that in a desired application. The DST of the complex fluids is simultaneously determined on the same timescale.

In this paper, we first validate our method with Newtonian fluids in order to define the lower and upper limits for viscosity measurements on drops of different sizes. We then measure dynamic properties of two practical examples of shear-thinning fluids: aqueous PEDOT:PSS solutions, used in the manufacture of organic electronic devices, and colloidal suspensions of a drug for use in pharmaceutical manufacturing. We show that the OD method is an effective rheometer for measuring the low amplitude dynamic viscosity in the period immediately after ejection from a nozzle and can be used to study thixotropy over much shorter timescales than in conventional rheometers.

2. Experimental Methods

2.1 *Dispensing and visualisation system for μL drops*

The μL drops are generated by liquid dispensing technology (LDT). A schematic diagram of the experimental arrangement for dispensing and visualisation of μL drops is shown in Fig. 1(a). The sample fluid is fed from a reservoir into a rotary piston pump head (IVEK-3A) driven by a digital servo drive (Allen-Bradley, Ultra3000) and rotary motor (Allen-Bradley, MPL-A230) controlled by Ultraware software. During the pump ejection cycle, the fluid is dispensed through a 15-cm long PTFE tube (Zeus) cut at a right angle to form a nozzle. AWG-15 tubing is used with an inner diameter of 1.45 ± 0.05 mm and an outer diameter of 2.25 ± 0.05 mm. The motor control parameters are adjusted to eject a single drop during each stroke of the piston. The stroke length is varied to control the drop volume. A Leica CLS 100× illuminator is used as a light source. It is collimated through a singlet lens with a focal length of 80 mm and a clear aperture of 20 mm. The drop formation and oscillation are

4

recorded by a high-speed CMOS camera (Photron FASTCAM-APX RS) with a Cosmicar television lens. The typical image size is 400 × 1024 pixels with a fixed frame rate of 2000 fps. The shutter exposure time of the CMOS camera is set to 5 μs. The camera is triggered via software. The output TTL signal from the camera is sent to the motor drive to start the pump. Measurements on drops were taken over approximately 8 different nozzle heights and the oscillation curves were stitched together over the overlapped position of the droplet from the images. A 3-mm diameter sapphire ball (tolerance of 2 μm) is used to calibrate the image and to check for image distortion. The apparent diameter of the sphere varied by less than ±1 μm over the central 80% of field of view of the camera; only this area was used in the data analysis.

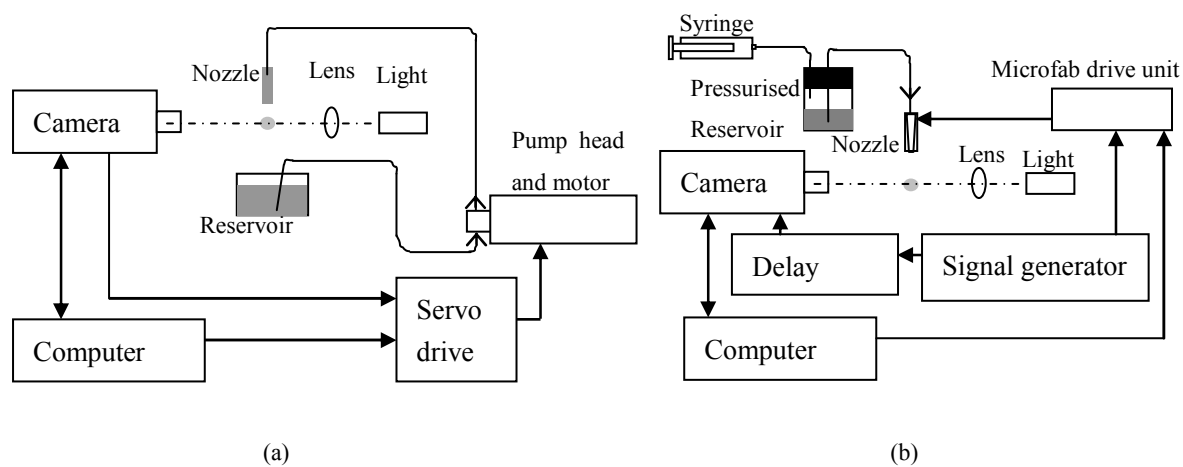(a)   (b)

FIG. 1 Schematic of the experimental arrangement for liquid dispensing and drop visualisation of (a) μL drop, and (b) pL droplet.

Ultra-pure water (Milli-Q A-10, Millipore) was used to calibrate the pump stroke volume, which is equal to the volume of a drop. For a fixed stroke length, we discard the first few drops and then count the pump strokes to generate 10 water drops. The drops are collected in a narrow-mouth glass bottle and weighted immediately with an analytical balance with readability of 0.1 mg. From the known density of water at the ambient temperature, the drop volume and hence the stroke volume can be determined. Figure 2 shows the measured stroke volume as a function of the nominal stroke length, measured with a digital dial meter (resolution of 0.01 mm) installed on the pump head. The data are fitted to a straight line through the origin with a slope of 2.55 ±0.01 μL/mm. Repeatability of 0.1% is obtainable once the stroke length is established.

2.2 *Dispensing and visualisation system for pL droplets*

Figure 1(b) shows a schematic diagram of the experimental arrangement for dispensing and visualization of pL droplets with a stroboscopic technique. Droplets with a typical volume of 100 pL are generated by a piezoelectric drop-on-demand (DoD) print-head (Microfab MJ-ABP-01, Horizon Instruments) controlled by a driver unit (Microfab CT-M3-02). The sample fluid is fed from a pressurised reservoir to a nozzle of diameter 40 or 80 μm until the meniscus of the fluid is observed at the orifice. A bipolar waveform is generally used and adjusted to eliminate satellites.
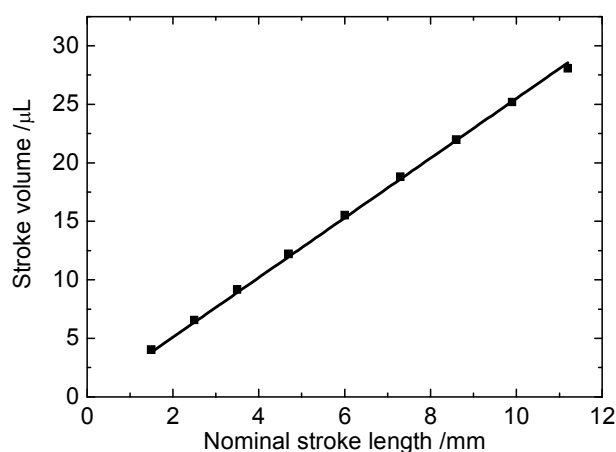

FIG. 2. Calibration of the stroke volume of water drops against stroke length. Solid square: experimental data. Line: linear fit through origin.

Shadowgraphs of the droplet are obtained with back illumination. The fast oscillatory motion of the droplet is visualized either with an ultra-high speed camera or with stroboscopic imaging. In the former case, a long duration (~ 2 ms), high-power, flash lamp illuminates the droplets through a light pipe with a lens, adjustable iris and light diffuser. A Shimadzu HPV-1 ultra-high-speed camera (EPSRC Engineering Instrument Pool) is used to record magnified images via a Navitar ×12 telescope with a ×10, 0.28 NA, Mitutoyo objective lens. The Shimadzu HPV-1 software is first primed for external trigger. A manual trigger is then applied to a pulse/delay generator which in turn triggers the Microfab drive controller, the Adept Electronics CU-500 flash power supply and controller and the HPV-1 camera. The HPV-1 exposure time used was 0.5 μs at both 1Mfps and 500kfps. The HPV-1 camera records a maximum of 102 frames at rates up to 10^6 fps. The pixel size was calibrated from images of long wires of known width of 104 μm. Droplets in flight were imaged until either the droplet exited the field of view of the camera or until the maximum number of frames of the high-speed camera had been recorded.

For the stroboscopic imaging, a blue LED is used as illuminator. A TTL signal generator triggers

the Microfab drive and, through a delay box, a CMOS camera (CamRecord CR450x3). A 12× zoom lens (LaVision) with attached 2× lens and 2× adapter tube is used as an image magnifier with spatial resolution of 1 μm. The image is calibrated with a calibration plate with array of dots 50 μm apart (LaVision) which gives us image resolution of 0.52 μm/pixel. For the imaging of droplets in flight, the camera exposure time is set to 1 μs. The resolution of the delay box is 0.1% of its range, i.e. 1 μs, which determines the temporal resolution of the strobe system. The delay is scanned to generate a pseudo-cinematographic sequence in which each frame is taken on a different drop.

2.3 *Image analysis*

The shape, volume and speed of the droplet were analysed through Matlab code with an edge detection algorithm using a Sobel operator. The reproducibility of drops was checked by stroboscopic imaging. For a fixed time delay, the position of the drop/droplets is within one pixel. The relative standard deviation of the measured drop volume is 0.5% for μL drops and 2% for pL droplets, which is mainly associated with image resolution and contrast.

2.4 *Sample preparation and characterisation*

Newtonian aqueous solutions were prepared with 1 wt% and 1.5 wt% hydroxyethyl cellulose (HEC, Aldrich, weight average molar mass M_w ~250,000 g mol^{-1}), 2.5 wt% hydroxypropyl cellulose (HPC-ssl, Nisso, M_w ~ 40,000 g mol^{-1}), and 5 wt% and 7 wt% hydroxypropyl cellulose (HPC-sl, Nisso, M_w ~ 100,000 g mol^{-1}). An AR 2000 rheometer (TA instrument) with a cone-plate geometry was used to measure the steady-state shear viscosity as a function of shear rate in the range 1–1500 s^{-1}. The equilibrium surface tension of the sample was measured by drop-shape analysis (FTA200, First Ten Ångstroms) with an accuracy of 0.5 mN m^{-1}. The density of the sample was derived from the mass of the sample in a 10-mL volumetric flask weighed by an analytical balance with readability of 0.1 mg. All measurements are performed under room temperature of 21±1 °C. TABLE I shows the average shear viscosity over the shear rate of 1–1500 s^{-1}, equilibrium surface tension and density of the Newtonian fluids. The viscosity of the cellulose solutions was almost independent of shear rate with an absolute variation of < 3 mPa s for HEC and < 0.7 mPa s for HPC fluids. HEC and HPC samples are surface-active and have a constant surface tension of 64.7±0.5 mN m^{-1} and 44.5±0.5 mN m^{-1}, respectively. For the oscillating drop measurement, HEC and HPC-sl solutions were used for the μL drops, while HPC-ssl solution and ultrapure water were used for pL droplets. The density, surface

tension and viscosity of water at 21 °C were obtained from Perry's Chemical Engineer Handbook.

TABLE I. Measured physical properties of cellulose solutions with different concentration

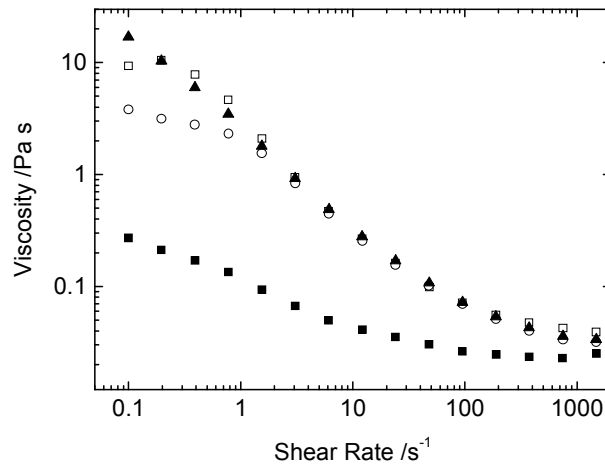| Sample	μ / mPa s	σ_{eq} / mN m^{-1} [a]	ρ / kg m^{-3} [b]
1% HEC	14±2	64.7	1003
1.5% HEC	27±3	64.7	1007
2.5% HPC-ssl	2.9±0.4	44.5	1002
5% HPC-sl	16.5±0.7	44.5	1005
7% HPC-sl	44.9±0.5	44.5	1010

[a] ±0.5 mN m^{-1}; [b] ±2 kg m^{-3}

The aqueous colloidal suspension contains HPC-ssl as a binder and viscosity modifier, fumed silica (DHK SiN20, Wacker) as a suspending agent, a surfactant (Tween 80, also known as polysorbate 80, Aldrich) as a dispersant and Griseofulvin (GF) (Shanghai Tech, micronised) as a model active pharmaceutical ingredient (API). Master formulae were first prepared. The soluble components (100 g, 20%wt HPCssl/water and 20 g, 10%wt Tween80/water) were stirred by magnetic bars at 40 °C until the solids were virtually dissolved. The master silica dispersion (200 g, 5% wt silica/water) was stirred with a magnetic bar for 2 hours at the rate of 500 rpm and then with an overhead mixer for 5 min at the rate of 1000 rpm. The silica suspension was then put into a bath sonicator for 30 min and stirred with a magnetic bar at the rate of 500 rpm for a further 5 hours. The master formulae were left for at least 12 h before final model colloidal suspensions were prepared. To make 50 g of the final colloidal suspension, the griseofulvin was weighed and wetted by the correct amount of the master Tween 80 solution and 2/3 of the required water. Under stirring, the appropriate amount of HPCssl and silica master formulae and finally the remaining water were gradually added. The suspension was stirred for a further 2 hours and sonicated for 15 min. All samples were weighed by a balance with an accuracy of 10 mg. Four suspensions were prepared with compositions shown in TABLE II. The suspension stability was checked by observation of the sedimentation rate of 7 mL of fluid in a 16-mm diameter sealed bottle over 5 days. Formulation GF-1, with the lowest SiN20 loading, is least stable with a sedimentation rate of 0.12 mm/hour, followed by GF-3 at 0.05 mm/hour. GF-2 and GF-4, with higher SiN20 loading, showed no sediment after 5 days. Before oscillating drop measurements, all suspensions were constantly stirred by a magnetic bar at a speed of 200 rpm. Measurements on the colloidal suspension were performed within one week of preparation and at room temperature of 21±1 °C.

TABLE II. Shear viscosity, μ, and density, ρ, of the colloidal suspensions. Compositions are given in wt%

Sample	HPC-ssl	SiN20	Tween 80	GF	μ @ 0.1 s^{-1} /mPa s	μ @ 1500 s^{-1} /mPa s	ρ /kg m^{-3} [a]
GF-1	7	0.5	0.5	5	0.27×10^3	23	1028
GF-2	5	1.7	0.5	20	9.3×10^3	39	1078
GF-3	5.5	1.5	0.5	15	3.8×10^3	30	1062
GF-4	7	2.5	0.5	5	17×10^3	31	1040

[a] ±2 kg m^{-3}

The steady-state shear viscosities are shown in Fig. 3(a). The high viscosity at low shear rate is associated with the formation of a hydrogen-bonded network between neighboring silica particles. The higher the SiN20 loading, the higher the viscosity at low shear. As the shear rate increases, the fumed silica network breaks down and the viscosity first decreases and then levels off at a shear rate of 1000 s^{-1}. The four suspension samples have a similar high shear viscosity. The steady-state shear viscosities at shear rates of 0.1 s^{-1} and 1500 s^{-1} are listed in TABLE II. The viscosity of the colloidal suspension GF-2 was checked over two weeks, showing no significant change. The dynamic viscosities, μ', of sample GF-2, -3 and -4 are shown in Fig. 3(b), with an oscillatory frequency sweep at strain amplitude below 0.4% to remain in the linear viscoelastic region, where $\mu'= G''/\omega$, G'' is loss modulus and ω is angular frequency. The linearity was checked at frequencies of 1 and 100 rad s^{-1}. We examined the Cox-Merz Rule[19] which correlates steady-state shear rheology with oscillating shear rheology at the same frequency. The steady-state viscosity is lower than the oscillatory equivalents which may be due to a larger loss of 'structure' at higher deformation.[20]
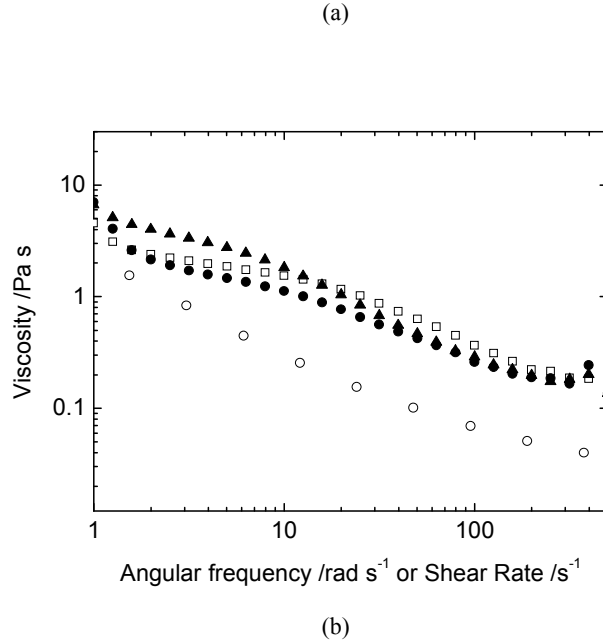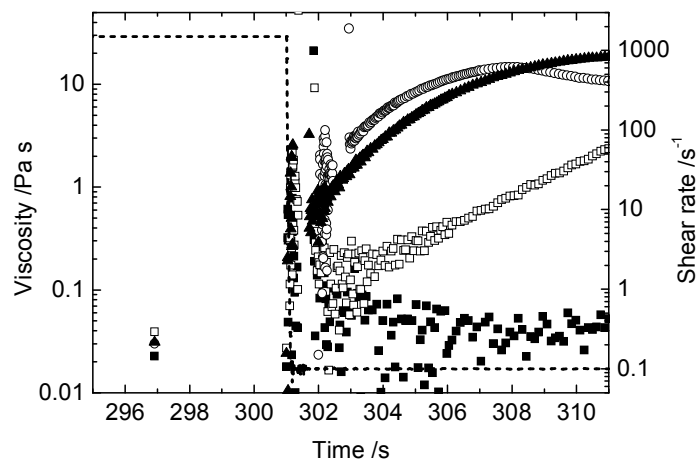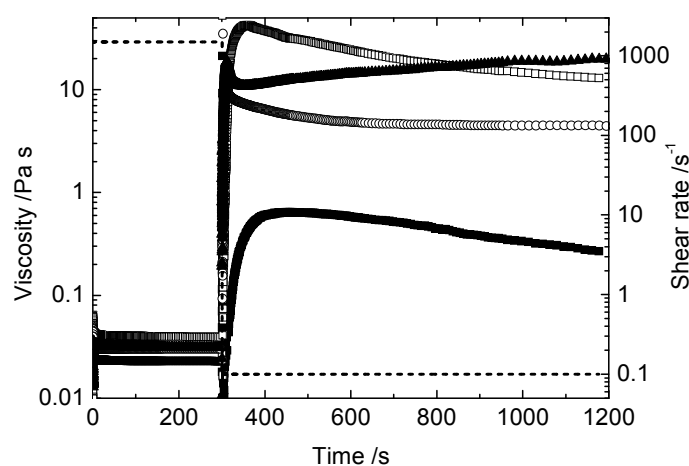
FIG. 3. (a) Steady-state shear viscosity of model pharmaceutical suspensions: GF-1 (solid square), GF-2 (open square), GF-3 (open circle) and GF-4 (solid triangle).(b) Dynamic shear viscosity of model pharmaceutical suspensions under oscillating shear, with abscissa in units of angular frequency: GF-2 (open square), GF-3 (solid circle) and GF-4 (solid triangle). For comparison, the steady-state shear viscosity of GF-3 (open circle) is also shown with the abscissa in units of shear rate.

We applied a two-step "peak-hold-flow" procedure with fast sampling in the rheometer to study the thixotropy of the model suspensions when the shear was switched from a high shear rate of 1500 s^{-1} to a low shear rate of 0.1 s^{-1}. This process mimics the shear history of a drop from the nozzle (high shear) to drop break-off (low shear). The response of the viscosity (Fig. 4) represents the recovery of the suspension network. Figure 4(a) shows how the viscosity responds for the first 10 s after the switch in shear rate. It takes about 200 ms for the rheometer motor to stabilize after the step in the shear rate. The viscosity data are very noisy for 1 s after the switch (Fig. 4(a)). By the time that the noise died away, the viscosity of the suspensions has recovered to some extent. GF-1, with the lowest SiN20 loading, recovers most slowly. Figure 4(b) shows the viscosity over a longer period after the switch in shear rate. All samples showed transient peaks in the viscosity response within ~100s after the switch the reason for which is not clear. Suspensions GF-1, -2 and -3 eventually relaxed to the equilibrium state, while GF-4 (with the highest SiN20 loading) quickly relaxed after the initial spike in viscosity and then slowly rebuilt its structure. Thus, all four suspensions are thixotropic, with the

10

fastest recovery of the network structure of GF-3 and GF-4.

(a)

(b)

FIG. 4. Viscosity response of colloidal suspensions to a switch in shear rate: viscosities of GF-1 (solid square), GF-2 (open square), GF-3 (open circle) and GF-4 (solid triangle). Variation in shear rate with time is shown by the dashed lines. (a) is the zoom-in of (b).

The equilibrium surface tensions of 0.5 wt% Tween 80, 5 wt% HPC-ssl, the mixture of 5 wt% HPC-ssl and 0.5 wt% Tween 80, and the colloidal suspensions were measured by drop-shape analysis (FTA 200). The samples that contain Tween 80 and a low GF loading (<5%) have equilibrium surface tension of 40.2 ±0.5 mN m^{-1} which is determined by the surfactant. 5 % HPC-ssl has an equilibrium surface tension of 44.5 ±0.5 mN m^{-1}. For higher GF loadings (GF-2 and -3), the apparent value of the surface tension is unexpectedly low; the value may be an experimental artifact arising from the high

11

solids content or may reflect weak surface activity of the GF particles.

The dynamic surface tension (DST) of 0.5 wt% Tween 80, 5 wt% HPC-ssl and the mixture of 5 wt% HPC-ssl and 0.5 wt% Tween 80 was measured by a maximum-bubble-pressure (MBP) tensiometer (SITA Dyno Messtechnik GmbH) for the bubble lifetime ranging from 15 ms to 2 s, shown in Fig. 5. The repeatability of the tensiometer is 0.5 mN m^{-1}. The tensiometer corrects for viscous and aerodynamic effects for fluids with the same viscosity as water, which in our case, is approximately the same as 0.5 wt% Tween 80. The DST of 5% HPC-ssl with and without Tween 80 is similar at short times, which indicates Tween 80 initially is not an important factor in lowering the DST. The apparent increase in the DST of 5% HPC-ssl and the mixture of 5% HPC-ssl and 0.5% Tween 80 at short times of < 200 ms is an artifact arising from the higher viscosity of the fluids (7 times that of the water calibration sample): absolute values of DST obtained from the Sita MBP tensiometer are not reliable for viscous complex fluids.
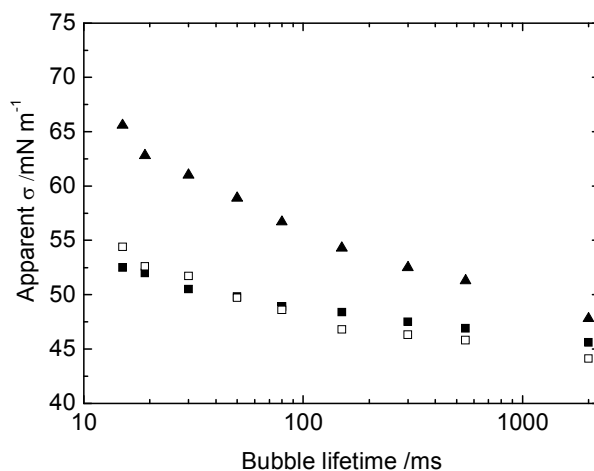

FIG. 5. Dynamic surface tension by maximum bubble pressure for 0.5 wt% Tween 80 (triangle), 5 wt% HPC-ssl (solid square) and the mixture of 5 wt% HPC-ssl and 0.5 wt% Tween 80 (open square).

The experiments with pL droplets used a commercial aqueous polymer dispersion poly(3,4-ethylenedioxythiophene): polystyrene-sulphonate (PEDOT:PSS, Heraeus Clevios). 0.7 wt% PEDOT:PSS was mixed with 0.06 wt% Dynol 607 surfactant (Air Products). The DST at 21°C approaches a constant value of 30 ± 2 mN m^{-1} at bubble lifetime of 15 s (Sita Pro-line 15 bubble tensiometer). Rheological measurements were performed at 25 °C with a parallel plate rotational rheometer at shear rates up to 4×10^4 s^{-1} and with a piezo axial vibrator (for details, see ref. 21). The shear viscosity falls from about 25 mPa s at a low shear rate of 1 s^{-1} to about 3.5 mPa s at the highest

measured shear rates of 4×10^4 s^{-1}. The relaxation time, λ, is estimated from $(\mu_0 + \mu_\infty)/2$ when $\lambda \dot{\gamma} = 1$,[22] i.e. at a shear rate λ^{-1}, where μ_0 is the viscosity in the initial Newtonian region, μ_∞ the viscosity in the second Newtonian region at high shear rates, and $\dot{\gamma}$ the shear rate. The relaxation time estimated by this method is about 10^{-3} s, showing weak elasticity.[21]

3. Results

The viscosity of the model suspensions is both shear and time-dependent. The transient viscosity of the fluids, which affects the jet/drop break-up and impact, depends on the shear history, which cannot be replicated on a commercial rheometer. Similarly, commercial instruments such as the MBP tensiometer cannot reliably measure the DST of viscous fluids on the relevant timescales (microsecond to milliseconds). Here we demonstrate that the oscillation of the free-falling drop in the LDT or DoD inkjet systems can itself be used to determine the transient viscosity and dynamic surface tension of the complex fluid on the timescale of a few tens of µs or ms, with the precise shear history experienced in a commercial application.

The deformation of a free-falling drop from its spherical shape is described by an infinite series of orthogonal surface spherical harmonics in Eq. 1. Expanding the Legendre polynomials up to the 4th order yields the following expression for the radius of the drop:

$$r(\theta,t) = a_0 \left[1 + \frac{1}{2} a_2(t)(3\cos^2\theta - 1) + a_3(t) \frac{5\cos^3\theta - 3\cos\theta}{2} + a_4(t) \frac{35\cos^4\theta - 30\cos^2\theta + 3}{8} + ... \right], \qquad (5)$$

where a_l is the instantaneous amplitude of the lth oscillation mode normalized by a_0. The oscillation modes conserve volume to first order in a_l and thus for small amplitude oscillations $a_0 = r_0$, the unperturbed drop radius. For larger oscillations one has to consider higher order terms and a_0 then varies with time according to $a_0(t)^3 = r_0^3 / [1 + 3\Sigma a_l(t)^2/(2l+1)]$.[1] We assume in our analysis that we can replace a_0 with r_0. We measure the polar (up-down) and equatorial (left-right) dimension of the drop, which are sensitive only to the even-order modes of oscillation. Equation (5) leads to a polar length $D_1 = 2r_0[1 + a_2(t) + a_4(t)]$ and an equatorial length $D_2 = 2r_0[1 - a_2(t)/2 + 3a_4(t)/8]$. The oscillation amplitude of the fundamental ($l = 2$) mode, $a_2(t)$, can be calculated from

$$a_2 = (3D_1 - 8D_2 + 10r_0)/(14r_0), \qquad (6)$$

and of the 4th order, $a_4(t)$, from

$$a_4 = 2(D_1 + 2D_2 - 6r_0)/(7r_0). \qquad (7)$$

If $a_4(t)$ is negligibly small, the amplitude of the fundamental mode $a_2(t)$ becomes

$$a_2 = (D_1 - D_2)/(3r_0). \tag{8}$$

The drop radius r_0 is determined from the drop volume in the LDT system or from the average value of D_1 and D_2 in the drop-on-demand inkjet system, where the error in $|D_1 - D_2|$ is less than one pixel with a typical image resolution of 0.5 μm/pixel.

We fit the dimensionless oscillation amplitude $a_2(t)$ to the functional form

$$a_2(t) = a_2(0) \cdot \exp(-t/\tau) \sin[2\pi t/T + \phi] + b_2, \tag{9}$$

where $a_2(0)$ is the oscillation amplitude at $t = 0$ (which is generally defined as the time when the recoiling ligament is readsorbed by the drop), τ is the oscillation decay time and T is the oscillation period from which we obtain $\Omega^* = 2\pi/T$. ϕ is the phase angle, b_2 is the eccentricity of the drop, which arises from imaging distortion or oblation of the droplets due to hydrodynamic effects. The oscillation amplitude of the 4th order mode decays 5 times faster than the fundamental mode according to Eq. (3). In our experiments, the 4th order mode is either negligibly small or is damped too quickly to use for the accurate determination of fluid properties. Once we know Ω^* and τ, we can calculate the dynamic surface tension and viscosity using Eqs. (2)-(4).
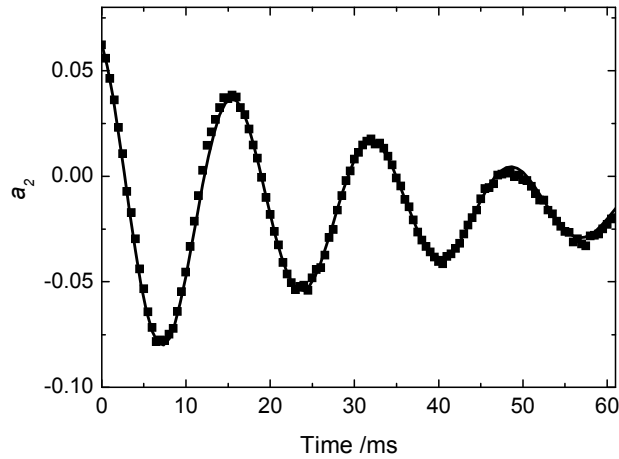
As our Newtonian fluids have well-defined surface tensions and shear viscosities, we first verify our experimental method by determining the surface tensions and viscosities of the Newtonian fluids by the OD method and comparing these values with those measured by a commercial tensiometer and rheometer. We then characterise the dynamic surface tension and transient viscosity of the drops formed from the non-Newtonian fluids.
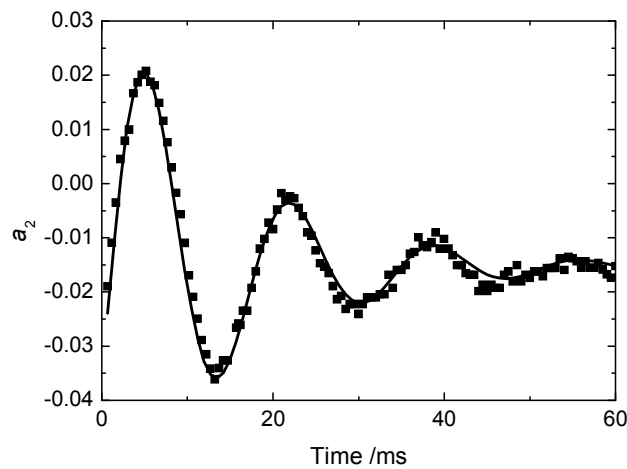
3.1 *Newtonian μL drops*

The LDT system was used to generate 15.3-μL drops of 1% and 1.5% HEC solutions and of 5% and 7% HPC-sl solutions. An error of 0.4% in drop volume is expected from the pump repeatability and the error in the density measurement used to determine the drop volume. The calculated drop radius is 1.540±0.002 mm. The oscillations of the drop were tracked until the oscillation amplitude was close to the image resolution.

For the Newtonian fluids, we analysed the oscillation amplitude from the point where a_4 reached the noise level to the point where a_2 reached the noise level. In this interval, a_2 takes the simple form of $(D_1 - D_2)/(3r_0)$. Figure 6 shows the oscillation amplitude of the fundamental mode averaged over
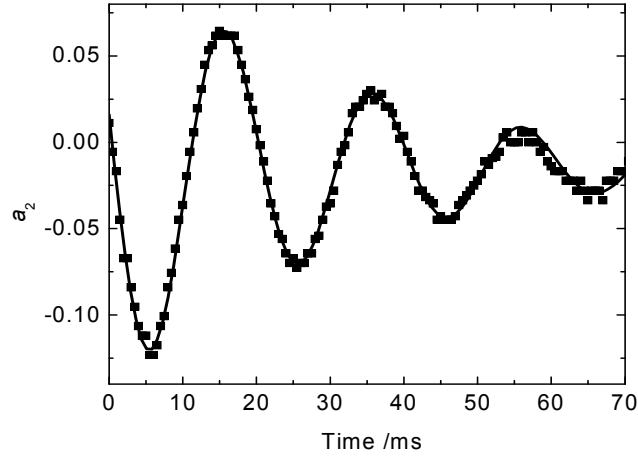
2–10 drops for each sample. The initial oscillation amplitude, $a_2(0)$, is less than 10% of the drop radius for which a linear theory is expected to hold.[15, 16] The surface tension and viscosity of the fluid were derived from Eqs. (2)-(4), respectively, on the assumption that they were invariant over the measured time interval. TABLE III compares the values of σ and μ obtained from oscillating drops with those measured by a commercial tensiometer and rheometer. The measurement errors are mainly propagated from 0.2% error in density, 0.13% error in drop radius, 0.5% error (maximum) in oscillation period, and 3% error (maximum) in decay time. As the drop radius is determined from the pump stroke volume rather than from an image with a typical resolution of 20 μm/pixel, the relative errors in surface tension and viscosity are significantly lower than for the picolitre droplets discussed below.
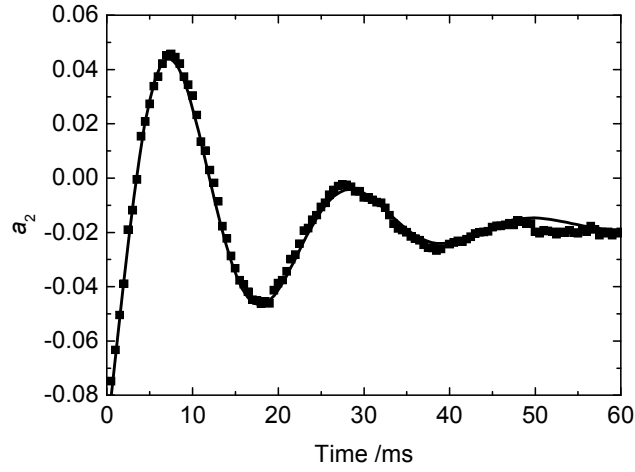

(a)

(b)

(c)

(d)

FIG. 6. Oscillation amplitude of 2nd order mode for aqueous solutions of (a) 1% HEC, (b) 1.5% HEC, (c) 5% HPC-sl, (d) 7%

HPC-sl. The lines are fits to Eq. (9).

TABLE III. Physical properties of Newtonian aqueous solutions obtained by a commercial tensiometer and rheometer, and

the measured surface tension and viscosity by the oscillating drop method

Sample	ρ /kg m^{-3}	Steady-state		Oscillating drop	
		σ_{eq}/mN m$^{-1\,a}$	μ/mPa s	σ/mN m^{-1}	μ / mPa s
1% HEC	1003	64.7	14±2	66.2±0.4	14.2±0.3
1.5% HEC	1007	64.7	27±3	66.3±0.7	31.3±0.9
5% HPC-sl	1005	44.5	16.5±0.7	45.1±0.4	14.9±0.4
7% HPC-sl	1010	44.5	44.9±0.5	43.2±0.4	34.3±0.6

[a] ±0.5 mN m^{-1}

The surface tension obtained by the OD method agrees with the tensiometric values for the HEC and HPC-sl samples to within experimental error (at the level of 2 standard deviations). The viscosities obtained by the OD method are also in agreement with the steady-state values except for 7% HPC-sl. The discrepancy in the 7% HPC-sl measurement may be due to the neglect of vorticity in the irrotational approximation that leads to Eqs. (2) and (3). The first three samples in TABLE III have an Ohnesorge number, $Oh = \mu/(\rho\sigma r_0)^{1/2}$ of ≤ 0.1. Prosperetti has shown that vorticity is generated in a viscous droplet by the free-moving surface during drop formation and that the irrotational approximation applies only when $Oh < 0.1$.[4] For the 7% HPC-sl solution, $Oh = 0.17$, which falls outside this range. Prosperetti found that, when vorticity is included, the decay rate of the oscillations is about 1.3 times slower than the irrotational result for $Oh \approx 0.2$. Consequently the viscosity determined by Eq. (3) will be ~1.3 times lower than true value, in agreement with our measurements.

3.2 *Newtonian pL drop*

The LDT device produces drops with μL volumes and timescales of a few tens of ms. Inkjets, on the other hand, eject much smaller droplets (pL volumes) at higher speeds and consequently the relevant timescales for the transient viscosity and surface tension are much shorter (tens of μs). To validate our imaging method for small droplets, we studied free-falling droplets (typical speed 0.5 m s^{-1}) of water and 2.5 % HPC-ssl generated by a Microfab DoD dispensing system with an 80-μm orifice. Figure 7 shows the oscillating water drop during the first three and half periods of measurement. To establish whether or not it is safe to neglect higher order modes, we calculated the fundamental oscillation amplitude, a_2 in two different ways: a_{2-1} is determined from Eq. (8) (neglecting the 4th-order mode) and a_{2-2} from Eq. (6) (allowing for the 4th-order mode). We also determined the 4th order oscillation amplitude, a_4, from Eq. (7). When a_4 approaches zero, a_{2-1} is expected to be equal to a_{2-2}. Figure 8 shows the experimental oscillation amplitudes of the two fluids and the best fit of a_{2-2} to a damped sine function. The 4th order results are offset for clarity. For water, the 4th order oscillation amplitude is negligibly small, the best fits for the oscillation period, T, and decay constant, τ, for a_{2-1} and a_{2-2} are indistinguishable. For example, the properties obtained from a_{2-1} and a_{2-2} are $T = 39.70 \pm 0.08$ μs and 39.66 ± 0.08 μs, respectively, and $\tau = 164 \pm 7$ μs and 163 ± 8 μs, respectively. The 4th order mode oscillation has a slightly higher amplitude for the HPC-ssl drop but the difference between the best fits to a_{2-1} and a_{2-2} is still within the error level. Using the oscillation

amplitude a_{2-2}, we obtain $T = 58.3 \pm 0.2$ μs and $\tau = 76.4 \pm 3.4$ μs for the 2.5 % HPC-ssl droplet. Oh = 0.02 and 0.08 for water and 2.5% HPC-ssl, respectively, which meets the criteria of Oh < 0.1 for the irrotational approximation to apply. The initial amplitude of oscillation in the fundamental mode is approximately 25% of the drop radius, where non-linear effects are expected to be negligible.[16] The surface tensions and viscosities derived from Eqs. (2)-(4) are listed in TABLE IV; the values obtained from the oscillating drop are in good agreement with those obtained from a commercial tensiometer and rheometer. The dominant contribution to the error in the DST is the radius, since it appears to the third power in Eq. (2), and the dominant contributions to the error in the viscosity are the radius (which appears to the second power in Eq. (3)) and the decay time. The measurement errors are mainly propagated from 1.7% error in drop radius and 5% error in decay time.
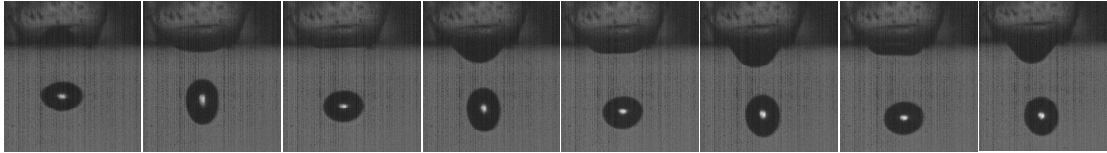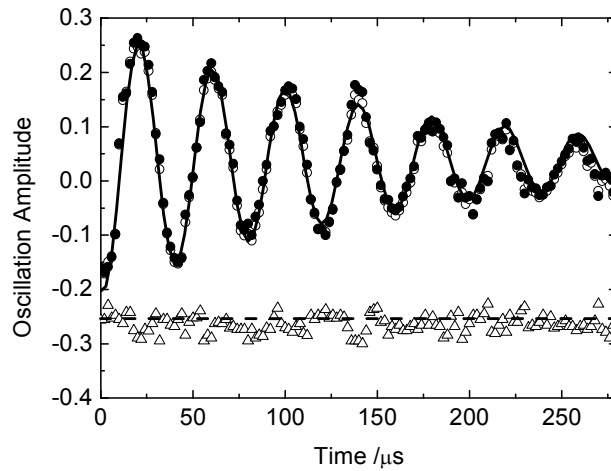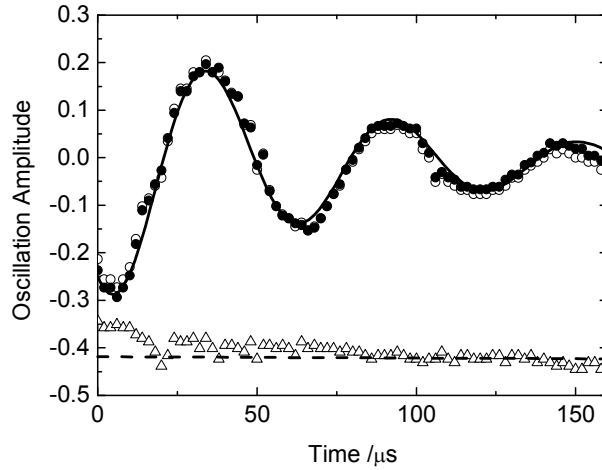

FIG. 7. Strobe images of water droplet with a radius of 28.2±0.5 μm. Time interval between frames = 20 μs.

(a)

18

(b)

FIG. 8. Oscillation amplitude of 2nd and 4th order modes, a_{2-1} (open circle), a_{2-2} (solid circle) and a_4 (open triangle) for (a) water droplet of radius 28.2±0.5 μm; (b) 2.5% HPC-ssl droplet of radius 30.5±0.5 μm. The solid lines are fits of a_{2-2} to Eq. 9. The dashed line is the zero for the 4th order mode, shown offset for clarity.

TABLE IV. Physical properties of water and 2.5% HPC-ssl obtained by a commercial tensiometer and rheometer, and the measured surface tension and viscosity by oscillating drop (OD)

Sample	Radius /μm [a]	ρ /kg m^{-3}	Steady-state		Oscillating drop	
			σ_{eq} /mN m^{-1} [b]	η /mPa s	σ /mN m^{-1}	η /mPa s
Water	28.2	998	72.4	0.980	70±4	0.97±0.04
2.5% HPC-ssl	30.5	1002	44.5	2.9±0.4	42±2	2.4±0.1

[a] ±0.5 μm; [b] ±0.5 mN m^{-1}

3.3 *Non-Newtonian μL drops*

The experiments described above were designed to validate our experimental rig with Newtonian fluids. In this and the following section we apply the methodology to colloidal suspensions with complex rheology, showing both strong shear-thinning and time-dependent behaviour. We first look at a pharmaceutical formulation for printing drugs onto placebo tablets. The 'Liquid Dispensing Technology' uses microlitre drops (~3 mm in diameter) ejected at low velocities which then accelerate under gravity before landing on a tablet less than 1 cm away from the nozzle. For the experiments here, we selected a stroke length to give a drop volume of approximately 18.8 μL and a drop radius of 1.650±0.002 mm. Figure 9 shows an image sequence of falling drop of sample GF-3 with 1.5 ms

19

between images. We start measuring the oscillation amplitude about 3 ms after drop break-off, once the recoiling ligament has been readsorbed by the drop. Figure 10 plots the amplitudes of the fundamental oscillation, a_{2-2}, and the 4th-order oscillation, a_4, for suspension GF-4. For these complex fluids, the amplitude of the 4th-order mode is significant for the first 20 ms, so it is preferable to use a_{2-2} to determine the viscosity and surface tension, rather than the simplified formula for a_{2-1} which neglects higher order oscillations. We illustrate the discrepancy by calculating the DST from both a_{2-2} and a_{2-1}. The respective surface tensions are 44.1±0.5 mN m^{-1} and 48.4±0.5 mN m^{-1}; the difference between the two values is well outside the calculated errors, with a_{2-1} significantly overestimating the DST.
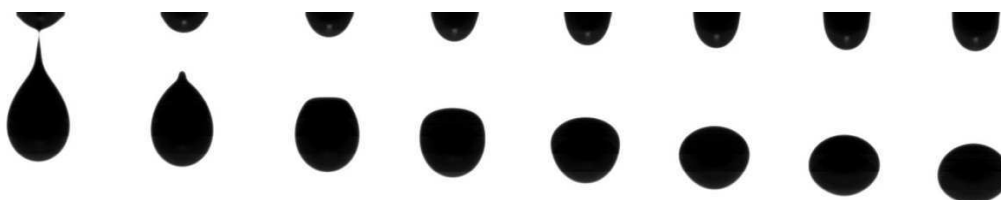

FIG. 9. Sequence of images of an 18.8-μL drop of a GF-3 suspension with a time interval of 1.5 ms between frames.

FIG. 10. 2nd and 4th order of oscillation amplitude of GF-4 suspension droplet. , a_{2-1} (open circle), a_{2-2} (solid circle) and a_4 (open triangle). The 4th order results were offset for clarity. The dashed line is the zero for the 4th order mode, shown offset for clarity.

The surface tension and viscosity for the four griseofulvin formulations obtained from a_{2-2} and Eqs. (2)-(4) are listed in TABLE V. As Tween 80 in suspensions initially (within a second) is not an

important factor in lowering the DST, we expect that the DST of all four suspensions on the measured timescale will be determined by the surface activity of the HPC and have a value of 44.5±0.5 mN m^{-1} as measured in Sec. 2.4. The surface tensions from the oscillating drop measurements are in reasonable agreement with this value for GF-1 and GF-4. However, for the drops with higher solid loading suspension (GF-2 and GF-3), the OD measurements give surface tensions up to 3.5 mN m^{-1} higher.

TABLE V also lists the steady-state viscosities at a low shear rate (0.1 s^{-1}) and at a high shear rate (1000 s^{-1}) of these strongly shear-thinning materials. The transient viscosities of all four suspensions are close to the high shear viscosities and one to three orders of magnitude less than the low shear viscosities. We note that according to the measured viscosity, the Ohnseorge number varies from 0.08 (GF-1) to 0.15 (GF-2). According to Prosperetti's analysis, the neglect of vorticity will lead to a systematic error of much less than 30% in the determination of the viscosity, even in the worst case (GF-2). We have neglected the role of elasticity (G′) on the shape oscillations, to which we will return at the end of the discussion.

TABLE V. Dynamic surface tensions and viscosities of Griseofulvin suspensions.

Sample	Density /kg m^{-3}	Steady-state		Oscillating drop	
		μ @ 0.1 s^{-1} /mPa s	μ @ 1500 s^{-1} /mPa s	σ /mN m^{-1}	μ /mPas
GF-1	1028	0.27×10^{3}	23	43.0±0.5	23±1
GF-2	1078	9.3×10^{3}	39	47.9±0.7	44±2
GF-3	1062	3.8×10^{3}	30	47.0±0.7	36±2
GF-4	1040	17×10^{3}	31	44.1±0.5	30±1

3.4 *Non-Newtonian pL droplets*

The sample solution for inkjet applications is a commercial formulation used in the printing of light-emitting displays. It is an aqueous suspension of 0.7 wt% PEDOT:PSS containing 0.06 wt% of the surfactant Dynol 607. The fluid was jetted at 21°C from a piezoelectric MicroFab print-head with a nominal diameter of 40 μm. The drop speed was about 4 m s^{-1}, towards the lower end of speeds used in commercial processes. Figure 11 shows the oscillation curves of a droplet 52.6 μm in diameter taken at frame rate of 1 MHz. Given the limited number of frames we can record, we commenced

measurement about 50 μs after drop formation, when the ligament had fully recoiled and the 4th order oscillation had been damped to noise level. Consequently, we analyse the oscillation with the simpler form, $a_{2\text{-}1} = (D_1–D_2)/(3r_0)$. The oscillation amplitude when we start recording is less than 5% of the drop radius, well within the linear regime. The best fit of the experimental data to a damped sine function yields $T = 36.6\pm0.1$ μs and $\tau = 37.5\pm1.2$ μs. Thus at 1 MHz frame rate, we can follow just under 3 full periods of oscillation. The dynamic surface tension and transient viscosity from Eqs. (2)-(4) are 68 ± 3 mN m^{-1} and 3.7 ± 0.4 mPa s, respectively. Note that these are average values over the time period of 50–150 μs after drop formation. The DST is much higher than the equilibrium value of 30 mN m^{-1}. The transient viscosity is close to the high-shear viscosity (3.5 mPa s at a shear rate of 5×10^4 s^{-1}) and much lower than the low-shear viscosity (25 mPa s at 1 s^{-1}).
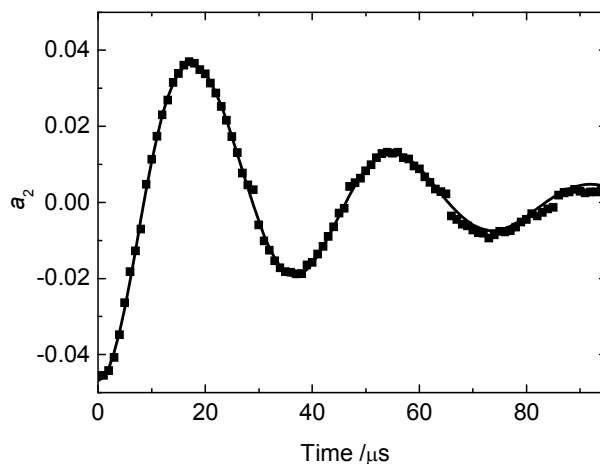

FIG. 11. Oscillation amplitude, $a_{2\text{-}1}$, of the fundamental mode for an 0.7% PEDOT:PSS solution. The line is a best fit to Eq. (9).

4. Discussion

4.1 *Droplet oscillation in Newtonian fluids*

The simplest model that can be used practically to model the free-oscillation of viscous drops is that of Lamb, in which the oscillation frequency and decay rate are given by Eqs. (2)-(4). Consequently, the surface tension and shear viscosity (both taken as constants) can be deduced from experimental measurements of the decay of the fundamental ($l = 2$) oscillation. Even for Newtonian fluids, however, there is a question of whether we can neglect higher-order oscillation modes, use a linear theory or neglect vorticity. For non-Newtonian formulations, additional complexities may arise from bulk

22

viscoelasticity and surface rheology. Consequently, it is important to validate our methodology first with Newtonian fluids before proceeding to real formulations with complex rheology.

Our measurement protocol, which measures the polar and equatorial dimensions of the drop, is sensitive only to even order modes of oscillation ($l = 2, 4, …$). The higher the order, the more rapidly the modes are damped (Eq. (3)). In particular, we note that the $l = 6$ mode is damped 2.4 times faster than the $l = 4$ mode so measuring the amplitude of the $l = 4$ mode will tell us when higher order modes may be safely neglected. We used two different formulae to determine the (time-varying) amplitude, a_2, of the fundamental mode, one of which allowed for the $l = 4$ oscillation and one which neglected it. We also measured the amplitude of the 4th-order mode, a_4. We found that for Newtonian fluids of both μL and pL drops, the fourth-order oscillation rapidly fell to noise level and that there was no significant difference between the two methods of analyzing the fundamental mode.

For the μL drops, the initial amplitude of oscillation (after retraction of the ligament following break-off of the drop) is less than 10% of the drop radius, so the linear theory is expected to work well. For the pL drops, we tested initial amplitudes up to 25% of the drop radius and found that the linear theory still gave a good fit to the experimental data with surface tensions and viscosities in agreement with the equilibrium values. This result also agrees with the conclusion of Becker *et al.* that nonlinear effects were most evident for higher oscillation modes ($l > 2$).[16]

The neglect of vorticity in Lamb's analysis was investigated by Prosperetti,[4] who showed that the irrotational approximation only held at low Ohnesorge numbers, Oh < 0.1. For Oh = 0.2, Lamb's formula overestimates the viscosity by about 30%. For the μL drops, we obtained good agreement between the shear rheometer and the oscillating drop (using the irrotational approximation) when Oh < 0.1 but at higher viscosity (Oh = 0.17) the OD method underestimated the shear viscosity by a quarter, in qualitative agreement with Prosperetti's predictions.

If we take Oh = 0.1 as the measurement upper limit for the use of the Eqs. (2)-(4), we obtain the constraint that the decay time τ should be $\geq 0.9T$. Solutions with higher values of Oh can still be measured, but the viscosity derived from Eq. (3) is only a qualitative guide – which may be all that is needed to distinguish between the high and low-shear behavior of non-Newtonian fluids. The viscosity cannot, however, be increased without limit. There is a critical Ohnesorge number of 0.57

where the oscillation frequency becomes zero and one no longer has an oscillating drop (Eq. (4)).

The lower limit on Oh is set more by practical than theoretical constraints. If $\tau \gg T$, then one needs to observe a large number of oscillations in order to determine τ accurately, which leads to a number of technical problems associated with the large field of view (and hence low pixel resolution), evaporation of volatile fluids during the measurement time, or the limited distance between the nozzle and the sample (when measurements are made on working machines). Low viscosity drops are also more prone to long-lived, high-order oscillations and non-axisymmetric deformations arising from asymmetric detachment (cf. 'tail-hooking' in inkjet printing). For ease of study, we recommend working with Oh > 0.03, i.e. $\tau < 3T$. Figure 12 plots the viscosities corresponding to Oh = 0.03 and 0.1 as a function of drop size, for a typical surface tension of 45 mN m^{-1} and density of 1×10^3 kg m^{-3}. For fundamental studies, the nozzle size should be selected so that the expected value of the fluid viscosity lies between the two curves. For practical applications, the viscosity will be dictated by the application. The viscosities in inkjet printing may exceed the upper line in Fig. 12, in which case Lamb's equations will only give approximate values. Corrections for higher Oh are given in ref. 18.
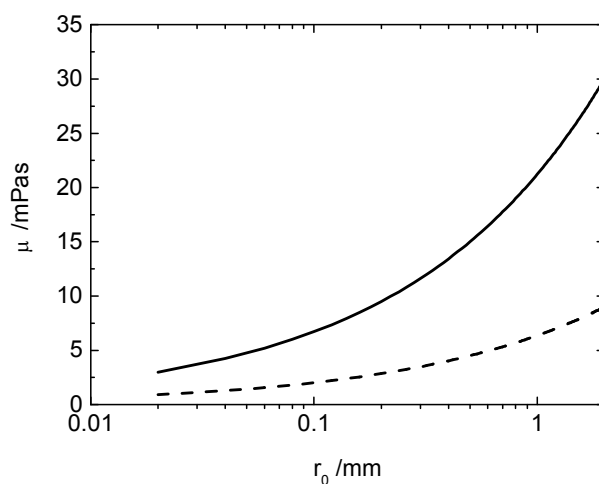

FIG. 12. Lower (dashed line) and upper (solid line) limit of viscosity of fluid for OD measurements for a surface tension of 45 mN m^{-1} and density of 1×10^3 kg m^{-3} as a function of drop radius, r_0.

4.2 μL drops of a pharmaceutical suspension

Having validated our experimental methodology on Newtonian fluids, we applied the technique to two complex fluids of industrial relevance. The first is a suspension of an active pharmaceutical ingredient (API) for use in the manufacture of pharmaceutical tablets by the LDT process. Four

formulations with a mass fraction of API between 5 and 20% were studied. All four suspensions exhibit strong shear thinning, with a low-shear (0.1 s⁻¹) viscosity of 0.3–20 Pa s and a high shear viscosity around 0.03 Pa s. Each suspension contains the surface-active polymer, HPC, at a high concentration (> 5wt%), so we would expect the dynamic surface tension (DST) to be close to the equilibrium value of 44.5 mN m⁻¹, which is indeed what we found experimentally from analysis of droplet oscillations. The higher order oscillations were more pronounced for the pharmaceutical suspensions than for the Newtonian HEC solutions and it was necessary to allow for the fourth-order mode in calculating the fundamental amplitude of oscillation, a_2. The first 5 ms after drop break-off are also likely to have a significant influence from modes with $l > 4$.

For the two formulations with the highest concentrations of the API (GF-2 and GF-3), the DST is 3 mN m⁻¹ higher than the equilibrium value, which is a significant difference based on our estimated errors. The suspension with the highest low-shear viscosity (GF-4), however, shows good agreement between the dynamic and equilibrium surface tensions. The reason for the small discrepancy for GF-2 and GF-3 is unclear.

In measurements of DST, reference is often made to the 'surface age' so it is helpful to consider what we mean by surface age in the context of OD measurements. We first estimate the mean surface expansion rate, θ, during drop formation from the surface area, A_0, of a pendant drop of 8 mm² to a full drop at break-off of $A = 32$ mm² occurring over a growth period of about 40 ms, i.e. $\theta = \ln(A/A_0)/\Delta t \approx 34\,\mathrm{s}^{-1}$. For a steady-state expansion, the surface age is given approximately by $1/(2\theta)$.[23] Consequently the surface age for a freshly created drop is ~15 ms. Once the drop has been formed, the percentage of newly created or destroyed surface (upon deviation from spherical) is small, so the surface age evolves at a similar rate as real time. The experimental measurements (see Fig. 10) were acquired from 2 to 30 ms after drop break-up i.e. at a surface age of approximately 17–45 ms. The average surface age corresponding to our measurement of the DST is thus about 30 ms. Turning to Fig. 5, we see that at surface age of 30 ms, the surfactant does not affect the DST of HPC solutions.

In order to understand the transient viscosity data, we consider the shear history of the fluid from inside the nozzle to the oscillating droplet. On the assumption of parabolic flow inside the nozzle, the average shear rate during the ejection of the drop is ~ 1×10^3 s⁻¹. Consequently, the fluid viscosity is close to the high shear rate plateau in Fig. 3(a) (μ ~ 30 mPa s). After the fluid leaves the nozzle, the droplet is no longer subject to wall stress and the shear rates inside the oscillating droplet are rather

low: an estimate of the velocity gradients inside the oscillating drop give shear rates well below 1 s^{-1}.[24] The corresponding viscosities under steady shear are 0.1–10 Pa s. Figure 4 gives information about the thixotropy of the fluid. Although there are no reliable measurements for the first 200 ms after the transition from high to low shear in the rheometer, it is clear that the time taken to rebuild the network of colloidal silica (many seconds) is long compared to the droplet age in the OD experiment (~ 30 ms). The suspension viscosities measured by the OD method agree to within experimental precision with the high-shear viscosities measured in the shear rheometer. They are much lower than the low-shear viscosities. They are also lower than the dynamic viscosity, μ', of ~ 200 mPas measured by oscillatory rheology for GF-2, -3 and -4 at an oscillation frequency of 200 rad s^{-1}, which corresponds to the oscillation period of the droplets of the order of 30 ms. The most probable explanation for these results is that the network of colloidal silica that is responsible for the high viscosity at low shear rates is destroyed in the high-shear environment of the nozzle and does not have time to rebuild on the timescale of the OD experiment.

The practical relevance of this observation is that behavior of the droplet during a LDT tablet printing process and impact and spreading on the pharmaceutical tablet (typically < 20 ms after drop formation) will be characterized by the high shear viscosity of the suspension and it is therefore this property that needs to be measured in formulating a new drug suspension.

4.3 *pL droplets of an inkjet formulation for organic electronics*

The second complex fluid we studied is an aqueous suspension of an organic electronic material (PEDOT:PSS) used in the manufacture of displays by inkjet printing. The formulation also contains a nonionic surfactant as a dispersant and wetting aid. The drop radius is two orders of magnitude smaller than those used in the LDT process and the oscillation period is three orders of magnitude shorter. This suspension is also shear-thinning, with the shear viscosity decreasing by an order of magnitude between shear rates of 1 s^{-1} and 10^4 s^{-1}. There are two salient results from the OD measurements: first, the DST is much closer to that of pure water than to the equilibrium surface tension of the suspension; second, the transient shear viscosity is characteristic of the high-shear viscosity, not the low-shear viscosity. We discuss each of these results in turn.

Dynol 607 (2, 5, 8, 11-tetramethyl 6 doecyn-5,8-diol ethoxylate) is a non-ionic gemini surfactant with a molecular weight of 310 g mol^{-1}. Its solubility in water is 0.032 wt%,[25] corresponding to a

solution concentration of about 1 mM. It does not form micelles.[25] The amount of Dynol 607 (0.06%) in the formulation exceeds the solubility limit, but some of the surfactant will be used to stabilise the PEDOT:PSS particles. For a nonionic surfactant with two branched chains, the maximum surface excess (corresponding to the minimum surface tension) is estimated to be $\Gamma_{max} \approx 2 \times 10^{-6}$ mol m^{-2}. If adsorption is diffusion-controlled, the diffusion time τ_d is defined as the mean time taken by a surfactant molecule to diffuse a distance given by the depletion length Γc,[26] where c is the bulk surfactant concentration:

$$\tau_d = \frac{1}{2D}\left(\frac{\Gamma}{c}\right)^2 .$$
(10)

A typical diffusion coefficient, D, for a low molecular weight surfactant in water is $D = 5 \times 10^{-10}$ m^2 s^{-1}, giving a value $\tau_d = 4$ ms. The time taken for a freshly formed surface to reach equilibrium is about $5\tau_d$, i.e. ~20 ms. The surface expansion rate during drop formation is of the order of 10^5 s^{-1}, giving a surface age of the freshly created drop of < 5 μs, which is negligible when compared to the drop flight time. The average surface age during the OD measurement is ~ 0.1 ms which is much shorter than surfactant diffusion time, $\tau_d = 4$ ms. Consequently, on the time-scale of the measurement, the surfactant does not have time to form an appreciable fraction of a monolayer and the resulting DST is close to that of pure water.

Within the nozzle, the PEDOT:PSS suspension is subject to high shear rates (>10^5 s^{-1}) and the droplet then emerges into a low shear environment. The velocity gradients within the oscillating drop are small (≤ 10 s^{-1}). The angular frequency of the oscillation is ~ 10^5 s^{-1} so the Cox-Merz Rule would predict a high shear viscosity. Unfortunately, we have no measurements on the thixotropy of the PEDOT:PSS suspensions on any timescale of relevance to inkjet printing. The PEDOT:PSS viscosity measured by the OD method is in agreement with the high rather than low shear viscosity.

4.4 *Role of elasticity*

Both the griseofulvin and PEDOT:PSS suspensions are viscoelastic at low shear. We have focused on the viscous contribution to the droplet oscillation, but what of elasticity? There is only a limited amount of work on elastic effects on drop oscillation. In 2001, Khismatullin and Nadim provided a detailed analysis of drop oscillations for the Jeffreys constitutive equation,[6] though most of the analysis concerned the simpler Maxwell Model. Recently, Brenn and Teichtmeister extended the work

of Khismatullin and Nadim with the objective of using the OD method to determine the deformation retardation time, λ_2, which appears in the Jeffreys equation.[18] While there is, a priori, no good reason why either of these models should accurately represent the colloidal suspensions studied here, the analysis of Khismatullin and Nadim does provide some useful insights into the present results. These authors define their Reynolds number as $Re = \rho \Omega_l r_0^2/\mu$ and divide their asymptotic analysis into the high and low Re limits. For our fluids, $Re = 30\text{–}40 \gg 1$ and $Oh \sim 0.1$ for both the griseofulvin and PEDOT:PSS suspensions (using the high-shear viscosity for μ). Khismatullin and Nadim numerically evaluated their expressions for oscillation frequency for a particular high Re (~241) and showed that the frequency was only very weakly dependent on the Deborah number $De = \lambda \Omega_l$ (where the relaxation time $\lambda = \mu/G'$ in the Maxwell model). Consequently, elasticity does not significantly affect our determination of the dynamic surface tension from Lamb's formula.

The influence of elasticity on the decay rate is more significant: for a Maxwell fluid the decay time increases substantially with increasing De even at high Re ,[6]

$$\tau_l = \frac{\rho r_0^2 (1 + De^2)}{\mu(l-1)(2l+1)},$$

(11)

Since it is only the portion of the stress that is in phase with the velocity that dampens the motion and therefore the viscosity that appears in the Lamb solution is μ', the real part of the complex viscosity. Consequently, for a Maxwell fluid the neglect of elasticity will underestimate both the low frequency viscosity and the modulus of the complex viscosity by $(1+De^2)$. A quantitative application of viscoelastic models to the data from our suspensions is complicated by the uncertainty in the interpretation of the relaxation times (λ_1 and λ_2, in the Jeffreys equation) for fluids where the non-Newtonian and thixotropic behavior arises from the breakdown and subsequent recovery of a particle network. The Jeffreys equation may not be the appropriate constitutive relationship. Fig. 4 shows that the time taken to rebuild the network of colloidal silica is long compared to the timescale in the OD experiment. Thus an interpretation of the OD data that neglects the effects of elasticity is consistent for the drug formulation in this paper, but there is clearly a need to explore further the influence of viscoelastic effects on drop oscillation in fluids that reversibly gel.[18]

5. Conclusion

The oscillating drop method provides a direct measurement of the dynamic surface tension and transient shear viscosity in drops formed in manufacturing processes involving nozzles or jets. We have used Newtonian fluids to validate experimental rigs for measuring oscillations of both μL and pL drops (corresponding to mm and 40-μm diameters) and established the range of Ohnesorge numbers ($\mu/(\rho\sigma r_0)^{1/2}$) over which accurate determination of the constitutive properties is practical. These limits correspond to a decay time, τ, for oscillation that is between 0.9 and three times the period of oscillation, T. The timescale for dynamic property measurement ranges from 10^{-5} to 10^{-2} s for drop volumes in the pL to μL range. We have shown that the oscillating drop method can also be applied successfully to complex fluids, showing strong shear-thinning and, in one case, a yield stress. The dynamic surface tension of the droplets can be understood in terms of the composition of the fluids and the rate of mass transfer of surface-active species to the nascent surface of the drops. The transient viscosities of the droplets were in all cases characteristic of the high shear rather than low shear rheology.

Acknowledgements

References:

1. Lord Rayleigh, On the capillary phenomena of jets. Proc. Roy. Soc. Lond. 29, 71-97 (1879)
2. H. Lamb, Hydrodynamics, 6th edn, pp. 473-475. Cambridge University Press (1932)
3. S. Chandrasekhar, The oscillations of a viscous liquid globe. Proc. Lond. Math. Soc. 9, 141-149 (1959)
4. A. Prosperetti, Free oscillations of drops and bubbles: the initial-value problem. J. Fluid Mech. 100, 333-347 (1980)
5. E. Becker, W. J. Hiller and T. A. Kowalewski, Nonlinear dynamics of viscous droplets. J. Fluid Mech. 258, 191-216 (1994)
6. D. B. Khismatullin and A. Nadim, Shape oscillations of a viscoelastic drop. Phys. Rev. E. 63,

061508 (2001)

7. R. S. Valentine, N. F. Sather and W. J. Heideger, The motion of drops in viscous media. Chem. Eng Sci. 20, 719-728 (1965)

8. G. D. Martin, S. D. Hoath and I. M. Hutchings, Inkjet printing - the physics of manipulating liquid jets and drops. J. Phys. 105, 012001:1-14 (2008).

9. C. Y. Wong, Limits on the nuclear viscosity coefficient in the liquid-drop model. Phys. Lett. B 61, 321-323 (1976)

10. A. R. Nelson and N. R. Gokhale, Oscillation frequencies of freely suspended water drops. J. Geophys. Res. 77, 2724-2727 (1972)

11. M. Ronay, Determination of the dynamic surface tension of liquids from the instability of excited capillary jets and from the oscillation frequency of drops issued from such jets. Proc. R. Soc. London A. 361, 181-206 (1978)

12. E. Trinh and T. G. Wang, Large-amplitude free and driven drop-shape oscillations experimental observations. J. Fluid Mech. 122, 315-338 (1982)

13. E. H. Trinh, P. L. Marston and J. L. Robey, Acoustic measurement of the surface tension of levitated drops. J. Colloid Interface Sci. 124, 95-103 (1988)

14. W. J. Hiller and T. A. Kowalewski, Surface tension measurements by the oscillating droplet method. Phys. Chem. Hydrodyn. 11, 103-112 (1989)

15. B. Stückrad, W. J. Hiller and T. A. Kowalewski, Measurement of dynamic surface tension by the oscillating droplet method. Exp. in Fluids. 15, 332-340 (1993)

16. E. Becker, W. J. Hiller, and T. A. Kowalewski, Experimental and theoretical investigation of large-amplitude oscillations of liquid droplets. J. Fluid Mech. 231, 189-210 (1991)

17. T. Matsumoto, T. Nakano, H. Fujii, M. Kamai and K. Nogi, Precise measurement of liquid viscosity and surface tension with an improved oscillating drop method, Phys. Rev. E 65, 031201 (2002)

18. G. Brenn and S. Teichtmeister, Linear shape oscillations and polymeric time scales of viscoelastic drops, J. Fluid Mech. 733, 504-527 (2013)

19. W. P. Cox and E. H. Merz, Correlation of dynamic and steady flow viscosity. *J. Polymer Sci.* 28, 619-622 (1958)

20. T. R. Al-Hadithi, H. A. Barnes and K. Walters, The relationship between the linear (oscillatory) and nonlinear (steady-state)flow properties of a series of polymer and colloidal systems, *Coll. Polymer Sci.,* 270, 40-46 (1992).

21. S. D. Hoath, S. Jung, W.-K. Hsiao and I. M. Hutchings, How PEDOT:PSS solutions produce satellite-free inkjets. Organic Electron. 13, 3259-3262 (2012)

22. M. M. Cross, Relation between viscoelasticity and shear-thinning behaviour in liquids, Rheol. Acta 18, 609-614 (1979)

23. C. D. Bain, The Overflowing Cylinder sixty years on, *Adv. Colloid Interface Sci.* 144, 4-12 (2008)

24. S. K. Chung and E. H. Trinh, Internal flow of an electrostatically levitated droplet undergoing resonant shape oscillation. Phys. Fluids 12, 249-251 (2000)

25. C.-M. Tåg, M. Juuti, K. Koivunen and P. A. C. Gane, Dynamic water transport in a pigmented porous coating medium: novel study of droplet absorption and evaporation by near-infrared spectroscopy, Ind. Eng. Chem. Res. 49, 4181-4189 (2010)

26. C. D. Taylor, D. S. Valkovska and C. D. Bain, A simple and rapid method for the determination of the surface equations of state and adsorption isotherms for efficient surfactants, Phys. Chem. Chem. Phys. 5, 4885-4891 (2003)